

# Nonparametric determination of the sign of $w+1$ in the equation of state of Dark Energy

*Houri Ziaeeepour*  
*Mullard Space Science Laboratory,*  
*Holmbury St. Mary, Dorking, Surrey RH5 6NT, UK.*  
*Email: hz@mssl.ucl.ac.uk*

## Abstract

We present a nonparametric method to determine the sign of  $w + 1$  in the equation of state of dark energy. It is based on geometrical behaviour and is more tolerant to uncertainties of other cosmological parameters than fitting methods. It permits to distinguish between different classes of dark energy models even with relatively low precision data. We apply this method to SNLS supernovae and to gold sample of re-analyzed supernovae data from Riess *et al.* 2004 [1]. Both data sets show strong indication of  $w < -1$ . If this result is confirmed by more extended and precise data available in near future, many of dark energy models, including simple cosmological constant, standard quintessence models without interaction between quintessence scalar field(s) and matter, and scaling models are ruled out.

Recent observations of SuperNovae (SN), Cosmic Microwave Background (CMB), and Large Scale Structures (LSS) indicate that the dominant content of the Universe is a mysterious energy with an equation of state very close to Einstein Cosmological Constant. The equation of state is defined by  $w$ , the ratio of pressure  $p$  to density  $\rho$ ,  $w = P/\rho$ . For a cosmological constant  $w = -1$ . The observed mean value of  $w$  for dark energy is very close to  $-1$ . Some of the most recent estimations are the followings: From combination of 3-year WMAP and SuperNova Legacy Survey (SNLS),  $w = -0.97_{-0.09}^{+0.07}$  [2]; from combination of 3-year WMAP, large scale structure and supernova data,  $w = -1.06_{-0.009}^{+0.016}$  [2]; from combination of CMAGIC supernovae analysis and baryon acoustic peak in SDSS galaxy clustering statistics at  $z = 0.35$ ,  $w = -1.21_{-0.12}^{+0.15}$  [3]; and finally from baryon acoustic peak alone  $w = -0.8 \pm 0.18$ . It is evident that with inclusion of one or two sigma uncertainty to measured mean values, the range of possible values for  $w$  runs across the critical value of  $-1$ . Moreover, in all these measurements the value of  $w$  depends on other cosmological parameters and their uncertainties in a complex way. Reconstruction methods for determining cosmological parameters from observations (see [4] and references therein for a review of methods) usually use fitting of continuous parameters on the data and determine a range for  $w$ .

On the other hand, the sign of  $\gamma \equiv w + 1$  is more crucial for distinguishing between various dark energy models than its exact value. For instance, if  $\gamma < 0$ , scalar field (quintessence) models with conventional kinetic energy and potential are ruled out because in these models  $\gamma$  is always positive. Decay of dark matter to dark energy [7] [8], or in general an interaction between these components can lead to an effective  $\gamma < 0$  without violating null energy condition [9] [10].

Here we propose a nonparametric method specially suitable for estimating the sign of  $\gamma$ . When the quality of data is adequate, the quantity  $A(z)$  defined in (2) can also be used to fit the data and to measure the value of  $\gamma$ . The expression *nonparametric* here is borrowed from signal processing literature where it means testing a null hypothesis against an alternative hypothesis by using a discrete condition such as jump, sign changing, etc., in contrast to constraining a continuous parameter (see e.g. [11]). We show that geometrical properties of  $A(z)$  are related to the sign of  $\gamma$  and we can detect it without fitting a continuous parameter.

The density of the Universe at redshift  $z$  is:

$$\frac{\rho(z)}{\rho_0} = \Omega_m(1+z)^3 + \Omega_h(1+z)^4 + \Omega_{de}(1+z)^{3\gamma} \quad (1)$$

where  $\rho(z)$  and  $\rho_0$  are total density at redshift  $z$  and in local Universe, respectively;  $\Omega_m$ ,  $\Omega_h$ , and  $\Omega_{de}$  are respectively cold and hot matter, and dark energy fraction in the total density at  $z = 0$ . We consider a flat universe in accordance with recent observations [2]. At low redshifts, the contribution of CMB to the total mass of the Universe is negligible. The contribution of neutrinos is  $\Omega_\nu h^2 = \sum m_\nu / 92.8 \text{ eV}$ ,  $h \equiv H_0 / 100 \text{ km Mpc}^{-1} \text{ sec}^{-1}$ , where  $H_0$  is present Hubble constant. The upper limit on the sum of masses of neutrinos from 3-year WMAP is  $\sum m_\nu < 0.62$  (95% confidence level) [13]. Therefore, for  $z < 1$  their contribution to the total mass of the Universe is  $\lesssim 4\%$  even if one of the neutrinos has very small mass and behaves as a warm dark matter. This is less than the uncertainty on the fraction of dark matter, and thus the approximation  $\Omega_m + \Omega_{de} \approx 1$  is justified. It can be easily shown that in this case:

$$\mathcal{A}(z) \equiv \frac{1}{3(1+z)^2 \rho_0} \frac{d\rho}{dz} - \Omega_m = \gamma \Omega_{de} (1+z)^{3(\gamma-1)} \quad (2)$$

Similar expressions can be obtained for non-standard cosmologies such as DGP [14] model and other string/brane inspired cosmologies [15]. It is also possible to find an expression similar to (2) for non-flat FLRW models and without neglecting hot matter. The left hand side would however depend on  $\Omega_k$ , and  $\Omega_h$  and would be more complex. Nonetheless, when the contribution of these components at low redshifts are much smaller than cold matter and dark energy, the general behaviour of  $\mathcal{A}(z)$  will be the same as approximate case studied here.

The right hand side of (2) has the same sign as  $\gamma$ . Moreover, the sign of its derivative is opposite to the sign of  $\gamma$  because due to the smallness of observed  $\gamma$ , the term  $\gamma - 1$  is negative. This means that  $\mathcal{A}(z)$  is a concave or convex function of redshift, respectively for positive or negative  $\gamma$ , see figure 1. In the case of a cosmological constant  $\mathcal{A}(z) = 0$  for all redshifts. This second feature of expression (2) is interesting because if  $\Omega_m$  is not correctly estimated,  $\mathcal{A}(z)$  will be shifted by a constant, but this will not modify geometrical properties of  $\mathcal{A}(z)$ .

The left side of expression (2) can be directly estimated from observations. More specifically,  $\Omega_m$  is determined from conjunction of CMB, LSS, and supernova type Ia data, and at present it is believed to be known with a precision of  $\sim 5\%$ . At low redshifts, the derivative of the density is best estimated from SN type Ia observations. In the case of FLRW cosmologies, the density and its derivative can be related to luminosity distance  $D_l$ , and its first and second derivatives:

$$\mathcal{B}(z) \equiv \frac{1}{3(1+z)^2 \rho_0} \frac{d\rho}{dz} = \frac{\frac{2}{1+z} \left( \frac{dD_l}{dz} - \frac{D_l}{1+z} \right) - \frac{d^2 D_l}{dz^2}}{\frac{3}{2} \left( \frac{dD_l}{dz} - \frac{D_l}{1+z} \right)^3} \quad (3)$$

$$D_l = (1+z)H_0 \int_0^z \frac{dz}{H(z)} \quad , \quad H^2(z) = \frac{8\pi G}{3} \rho(z) \quad (4)$$

It is remarkable that the right hand side of (3) depends only on one cosmological parameter,  $H_0$ . Nonetheless, similar to an uncertainty on  $\Omega_m$ ,  $H_0$  scales  $\mathcal{B}(z)$  similarly at all redshifts, and therefore it does not change the overall geometrical properties  $\mathcal{B}(z)$  and  $\mathcal{A}(z)$ .  $D_l$  can be directly obtained from observed luminosity of standard candles such as supernovae type Ia. In the case of LSS observations where the measured quantity is the evolution of density  $\rho$  with redshift,  $\mathcal{B}(z)$  is measured directly up to an overall scaling by  $\rho_0$ . This does not change the geometrical properties of  $\mathcal{B}(z)$  and  $\mathcal{A}(z)$ , i.e. the scaling by a positive constant does not flip a convex curve to concave or vis-versa.

In summary, uncertainties of  $\Omega_m$  and  $H_0$  do not affect the detection of the sign of  $\gamma$  through geometrical properties of  $\mathcal{A}(z)$ . This is quite different from fitting methods. They are sensitive to all numerical parameters  $H_0$ ,  $\Omega_m$ ,  $\Omega_{de}$ , and  $w$  in a complex way, usually through a non-linear equation such as chi-square or likelihood equation, and it is very difficult to assess the effect of uncertainty of one parameter on the estimation of others, and more specifically on the determination of the sign of  $\gamma$ .

When this sign detection method is applied to standard candle data such as supernovae type Ia where the measured values are related to  $D_l$ , according to (3), one has to calculate first and second derivative of  $D_l$ . Numerical calculation of derivatives is not trivial. To have a stable and enough precise result, not only the data must have high resolution and low scatter, but also it is necessary to smooth them.

To test the stability of numerical calculation and the method in general, we also apply it to simulated data. The details of numerical methods is discussed in the Appendix.

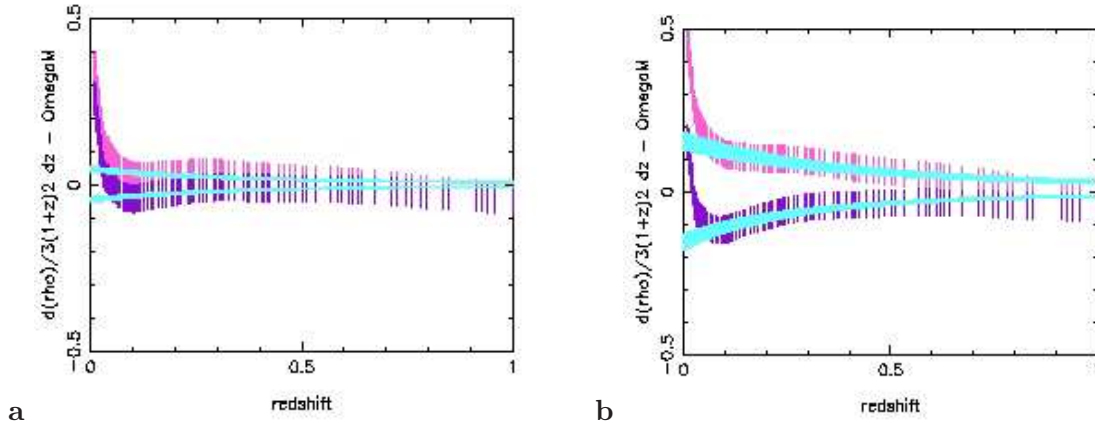


Figure 1:  $\mathcal{A}(z)$  in Eq.(2) as a function of redshift; **a**:  $\gamma = \pm 0.06$  (corresponding to best fit of 3-year WMAP, LSS, and SN data [2]) and **b**:  $\gamma = \pm 0.2$  (corresponding to best fit of 3-year WMAP and CMAGIC SN data [3]). For both plots  $H_0 = 73 \text{ km Mpc}^{-1} \text{ sec}^{-1}$  and  $\Omega_{de} = 0.77$ . We consider 5% of uncertainty for both quantities. Blue curves present right hand side of (2), including the uncertainty on the value of  $\Omega_{de}$ . Curves decreasing or increasing with increasing redshift present respectively positive and negative  $\gamma$ . Magenta and purple curves present numerical determination of  $\mathcal{A}(z)$  respectively for positive and negative  $\gamma$  from about 150 simulated supernovae distributed with uniform probability in  $\log(z)$ . These plots show that numerical errors dominate near two boundaries of the redshift range. It is also evident that with this method one can distinguish between positive and negative  $\gamma$  for  $|\gamma| \gtrsim 0.06$ .

Two examples of reconstruction of simulated data are shown in Fig.1. It is evident that despite deformation of the reconstructed curves due to numerical errors and uncertainties, the difference between convexity of curves for positive and negative  $\gamma$  is mostly preserved and can be used visually or by using a slope detection algorithm to find the sign of  $\gamma$ . The simulated data is however much more uniform than presently available data, see Fig.2. Although for mid-range redshifts the data follow a curve similar to what is expected from FLRW cosmologies, artifacts appear close to boundaries and at high redshifts where the quality of data is worse. Moreover, visual inspections or slope detection lack a quantitative estimation of uncertainty of measured sign for  $\gamma$ . Another complexity of this cosmological sign detection problem is that not only the observable  $\mathcal{A}(z)$  is noisy, it also varies. In signal processing, in most practically interesting cases the signal is constant but noisy. Therefore, usual binomial estimation of the probability or optimization of detection [12] are not applicable.

Here we take another strategy, specially suitable for this cosmological sign detection task. The null hypothesis for dark energy is  $\gamma = 0$ . Assuming a Gaussian distribution for uncertainty of reconstructed  $\mathcal{A}(z)$  from data and from simulated data for  $\gamma = 0$  model, for each data-point we calculate the probability that the data-point belongs to the null hypothesis. To include the uncertainty of data, we integrate the uncertainty distribution from  $-\sigma$  to  $+\sigma$  around the mean value:

$$P_i = \frac{1}{\sqrt{2\pi(\sigma_{0i}^2 + \sigma_i^2)}} \int_{\mathcal{A}_i - \sigma_i}^{\mathcal{A}_i + \sigma_i} dx e^{-\frac{(x - \mathcal{A}_{0i})^2}{2(\sigma_{0i}^2 + \sigma_i^2)}} \quad (5)$$

where  $\mathcal{A}_i$  and  $\sigma_i$  are from  $i^{th}$  data-point, and  $\mathcal{A}_{0i}$  and  $\sigma_{0i}$  from simulated null hypothesis model at the same redshift. Averaging over  $P_i$  gives  $\bar{P}$ , an overall probability that the dataset corresponds to the null hypothesis. As  $\gamma = 0$  is the limit case for  $\gamma > 0$ ,  $\bar{P}$  is also the maximum probability of  $\gamma > 0$ .

We have applied this sign detection algorithm to two supernova datasets: published data from Supernova Legacy Survey (SNLS) [5] and low redshift supernovae ( $z < 0.45$ ) of gold sample of re-analyzed

supernovae data by Riess *et al.* 2004 [1]. The reason for using only the low redshift subset of the latter compilation is that the scatter and uncertainty of the peak magnitude at higher redshifts is too large, and with numerical methods used in this work, it is not possible to recover a reasonably stable and smooth distribution for  $\mathcal{A}(z)$ .

Fig.2 shows  $\mathcal{A}(z)$  obtained from these data. To estimate the effect of the reconstruction, we compare  $\mathcal{A}(z)$  from data with simulated data as described in the caption of Fig.2. Simulated standard sources are at the same redshifts as in the datasets to make simulated samples as similar to data as possible.

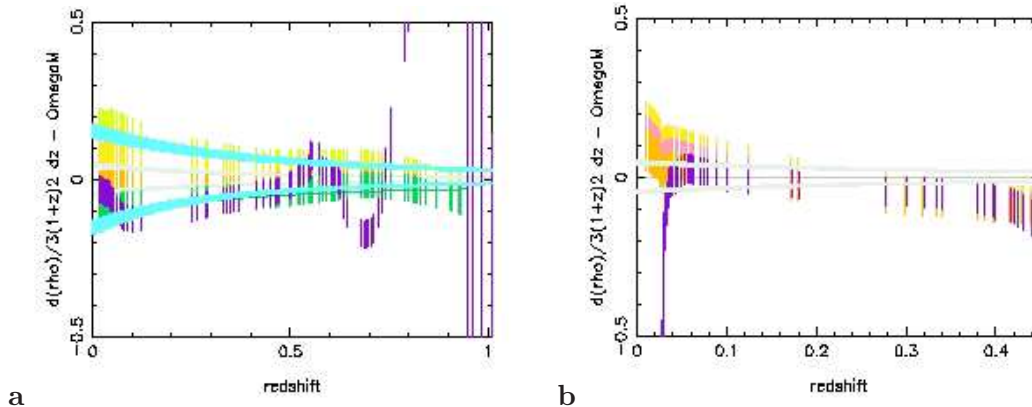


Figure 2:  $\mathcal{A}(z)$  from: 117 supernovae of the SNLS data (**a**-purple curve), and 88 supernovae with  $z < 0.45$  recompiled and re-analyzed by Riess *et al.* 2004 [1] (**b**-purple curve). Error bars present 1-sigma uncertainty. In (**a**), green, orange, yellow, and light green curves present the reconstruction of  $\mathcal{A}(z)$  from simulations for  $\gamma = -0.2, -0.06, 0.6, 0.2$ , respectively. The overall probability of null hypothesis ( $\gamma = 0$ ) is  $\bar{P} = 0.27$ , therefore the probability of  $\gamma < 0$ ,  $1 - \bar{P} = 0.73$ . Light grey and cyan curves are theoretical calculation including the uncertainty on  $\Omega_{de}$ , respectively for  $\gamma = \pm 0.06, \pm 0.2$ . In (**b**), the pink curve presents simulated distribution for  $\gamma = 0$  - a cosmological constant. For this dataset  $1 - \bar{P} = 0.75$ . The dark grey straight line is the theoretical expectation for  $\mathcal{A}(z)$  when dark energy is a cosmological constant. Definition of other curves are the same as (**a**).

In both datasets the probability of  $\gamma \lesssim 0$  or equivalently  $w \lesssim -1$  is larger than 70%. The SNLS data is consistent with a  $\gamma$  as small as  $\sim -0.2$ <sup>1</sup>. There are however significant deviations from a smooth distribution for  $z \lesssim 0.1$  and  $z \gtrsim 0.5$ . We attribute them to relatively large scatter of the data at these redshifts that makes reconstruction instable, see Fig.3-a.

To see whether the large negative  $\gamma$  concluded from the SNLS data is due to the data scattering and/or reconstruction algorithm artifacts, we also apply the same formalism to a subset of these data with  $z < 0.45$ . The result is shown in Fig.3-b along with simulations in the same redshift range. The *bump* at very low redshift in Fig.2 does not exist in this plot, and therefore we conclude that it is an artifact of numerical calculation. Although  $\mathcal{A}(z)$  distribution in this data set is also convex and the probability of  $\gamma < 0$  is  $> 90\%$ , it does not have the same slope as any of models. More specifically, it seems that low and high redshift sections of the curve correspond to different values of  $\gamma$ . For  $z \lesssim 0.15$ ,  $\mathcal{A}(z)$  is close to theoretical and simulated data with  $\gamma = -0.2$ . For  $z \gtrsim 0.25$ ,  $\mathcal{A}(z)$  approaches the values for larger and even positive  $\gamma$ . Such behaviour does not appear in Fig.2. Giving the fact that the number of available data points with  $z \gtrsim 0.25$  in this subset is small the most plausible explanation is simply numerical artifacts. Alternative explanations are evolution of  $\gamma$  with redshift and an under-estimation of  $\Omega_m$ , see Eq.(2). If the latter case is true, the value of  $\gamma$  must be even smaller than  $-0.2$ . With a data gap in  $0.15 \lesssim z \lesssim 0.25$  interval and a small total number of entries in this data set- only 58 supernovae - it is not possible to make any definite conclusion about the behaviour of this data. We should also mention that nearby SNe with  $z < 0.25$ , intermediate SNe  $0.25 < z < 0.4$ , and high redshifts ones

<sup>1</sup>As the main purpose of this paper is determination of the sign of  $\gamma$ , we don't perform any fitting to obtain its values. Estimation of values here are from plots.

$z > 0.4$  in SNLS are not completely treated in the same way [5]. It is therefore possible that some of the observed features explained here are purely artifacts of the analysis of raw observations.

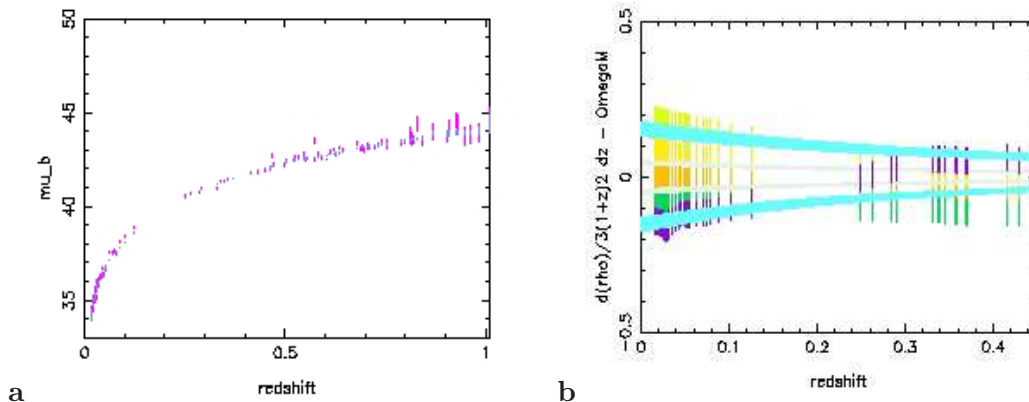


Figure 3: **a:**  $\mu_b$  distribution of SNLS supernovae, data (magenta), smoothed distribution by the method explained in the Appendix (blue). Although this distribution look quite smooth, even small sudden variations can lead to large variations in derivatives. **b:**  $\mathcal{A}(z)$  for SNLS supernovae with  $z < 0.45$ . definition of curves is the same as in Fig.2. For this dataset  $1 - \bar{P} = 0.93$  when cosmological parameters are the same as Fig.2. If  $\Omega_{de} = 0.73$  is used,  $1 - \bar{P} = 0.96$  for the same data.

Fig.2-b shows  $\mathcal{A}(z)$  determined from gold sample supernovae recompiled by Riess, *et al.* [1]. This dataset is consistent with  $\gamma < 0$  with a probability  $\sim 75\%$  at 1-sigma and  $\sim 66\%$  at 2-sigma. This plot also shows that the value of  $\gamma$  estimated from this data is  $\sim -0.06$ , larger than estimation from SNLS data.

The reason for the difference between estimated values for  $\gamma$  from SNLS and Riess, *et al.* compilation is not clear because the value of  $w$  reported in Ref. [1] and Ref [5] are consistent. Nonetheless, the estimated values here are in the range reported by other works [2] [3]. The difference between results of two datasets is most probably related to their different scatter and uncertainty, and the fact that low and high redshift data are not treated in the same way. We should also mention that recent claims about contamination of supernova type Ic and the effect of asymmetric explosion in the lightcurve of supernova type Ia [16], and possible differences between low and high redshift supernovae [17] can not explain the difference between the results of these datasets. These phenomena affect both surveys in the same way. Despite these discrepancies and uncertainties, both datasets are in good agreement about negative sign of  $\gamma$ .

The results of present study show various shortcomings in both datasets used here. Our first remark is the large gap in redshift distribution of observed supernovae in redshift range  $0.1 \lesssim z \lesssim 0.3$ . Both datasets have less than 6 supernovae in this range and nothing in  $0.15 \lesssim z \lesssim 0.25$ . This is not an important issue for finding redshift distribution of  $D_l$ , but redshift gap becomes very important when derivatives of  $D_l$  are calculated. The lack or rareness of supernovae data in this redshift range is related partly to the history of star formation in galaxies [18], and partly to optimization of surveys [19] for detection of very low or high redshift supernovae which decreases the probability of detection of mid-range SNe. A systematic survey of galaxies in this range is therefore necessary to fill the present gap. Sloan Supernova Survey [20] is optimized to detect SNe in  $0.1 \lesssim z \lesssim 0.35$  and should provide the missing data in near future.

Our second observation is a large scatter in both datasets around redshift  $\sim 0.55$ , see Fig.3-a. This leads to a large scatter in the numerical determination of derivatives in (3) and makes the results unusable, see Fig.2-a. In future observations the reason of this large scatter should be understood, and if possible reduced. From theoretical calculation and simulations shown in Fig.2 one can also conclude that with present uncertainties of cosmological parameters, the most important redshift range for determining the equation of state of dark energy is  $z \lesssim 0.8$ . Although the technical challenge,

understanding of physics of supernovae [17] and their evolution, and applications for other astronomical ends make the search of supernovae at larger distances interesting, they will not be in much use for determining the equation of state of dark energy, at least not at lowest level which is the determination of redshift independent component of  $w$ .

On the other hand, improvements in numerical techniques and algorithms would lead to better measurements. One of the possibilities in this direction is the application of an adaptive smoothing algorithm with variable degrees of smoothing depending on the amount of scattering in the data. More sophisticated smoothing algorithm also has been proposed [21]. We postpone the application these more advanced methods to future, when a larger data set becomes available.

In summary, we have proposed a nonparametric formalism to investigate the sign of  $\gamma$  in the evolution equation of dark energy. When better quality data become available fitting can be added to this method to find the value of  $\gamma$  and not just its sign. The advantage of this method with respect to multi-parameter fitting is that the dependence on cosmological parameters is explicit, and therefore it is easier to assess the effect of their uncertainties on the measurements. This method is specially suitable for applying to supernova data where the standard observable - the peak magnitude - can be directly related to cosmological distance, and thereby to cosmological variation of total density. It can also be applied to data from galaxy clustering surveys which permit to determine the variation of average density of the Universe with redshift, but not to integrated observables such as CMB anisotropy. By applying this method to two of largest publicly available supernovae data sets we showed that they are consistent with a  $w < -1$ . Present data is not however enough precise to permit the estimation of  $|w|$  with good certainty. With on-going projects such as SNLS, Supernova Cosmology Project [22], and SDSS SNe survey, and future projects such as SNAP and DUNE, enough precise datasets should be available in the near future.

**Appendix:** To calculate  $\mathcal{A}(z)$  in (2) for standard candles we must determine the luminosity distance. It is related to the magnitude of the standard candle:  $D_l/D_0 = 10^{\mu_b/5}$ , where  $D_0$  is the distance for which the common luminosity of standard sources is determined from theoretical models or observations. The standard magnitude at a given distance depends on  $H_0$  and a correction must be added if a different  $H_0$  is used in the calculation of  $\mu_b$  [5]. For simulating the data  $D_l$  is calculated from (4) and the relation above is used to determine the corresponding  $\mu_b$  to which we add a random uncertainty with a standard deviation of 3%. From this point the same procedure is applied to both simulated and real data to determine  $\mathcal{A}(z)$ .

Expression (3) for  $\mathcal{B}(z)$  contains first and second derivatives of  $D_l$  which must be calculated numerically from data. It is however well known that direct determination of derivatives leads to large and unacceptable deviation from exact values. One of the most popular alternative methods to the direct calculation is fitting of a polynomial around each data point and then calculating an analytical derivative using the polynomial approximation in place of the data. We use this approach to determine derivatives of  $\mu_b$  and  $D_l$ . In addition, before applying this approach, we smooth the distribution of magnitudes using again the same polynomial fitting algorithm.

In FLRW cosmologies the redshift evolution of the luminosity distance is very smooth. Therefore, a second order polynomial for smoothing is adequate. Fitting is based on a right-left symmetric, least  $\chi^2$  algorithm, and we have implemented *lfit* function of Numerical Recipes [23] for this purpose. By trial and error we find that 19 data-point fitting gives the most optimal results regarding the number of available data points and their scatter. Close to boundaries however less data point for fitting is available in one side of each point, and therefore the fitting is less precise. The artifacts discussed above are mostly related to this imprecision of numerical calculation. In the present work no adaptive smoothing is applied. In addition to smoothed data and their derivatives, the function *lfit* calculates a covariant matrix for uncertainty of parameters (derivatives). We use diagonal elements as 1-sigma uncertainty of the smoothed data and its derivatives. The uncertainty of  $\mathcal{A}(z)$  is calculated from the uncertainty of terms in (2) and (3) using error propagation relation: For  $f(x_1, x_2, \dots)$ ,  $\sigma_f^2 = \sum_i \sigma_{x_i}^2 (\partial f / \partial x_i)^2$ . Smoothed terms and parameters in  $\mathcal{A}(z)$  are considered as independent

variables with their own uncertainty.

## References

- [1] A.G. Riess, *et al.*, *ApJ*. **607**, (2004) 665, astro-ph/0402512.
- [2] D.N. Spergel, *et al.*, astro-ph/0603449.
- [3] A. Conley, *et al.*, *ApJ*. **644**, (2006) 1, astro-ph/0602411.
- [4] V. Sahni, A. Strarobinsky, astro-ph/0610026.
- [5] P. Astier, *et al.*, *A. & A.* **447**, (2006) 31, astro-ph/0510447.
- [6] D.J. Eisenstein, *et al.*, *ApJ*. **633**, (2005) 560, astro-ph/0501171.
- [7] H. Ziaepour, astro-ph/0002400.
- [8] H. Ziaepour, *Phys. Rev. D* **69**, (2004) 063512, astro-ph/0308515.
- [9] S. Das, P.S. Corasaniti, J. Khoury, *Phys. Rev. D* **73**, (2006) 083509, astro-ph/0510628.
- [10] H. Ziaepour, hep-ph/0603125.
- [11] E.L. Lehmann, H.J.M. Dabrera, *Nonparametrics*, Holden-Day, San Fransisco, CA, 1975, J.M. Moriss, *IEEE Trans. Comm.* **39**, (1991) 1726.
- [12] H. Gil Kim, *et al.*, IEEE MILCOM 97 Proceedings, Vol. 3, (1997), 1382.
- [13] S.Hannestad, G.G. Raffelt, astro-ph/0607101.
- [14] G. Dvali, G. Gabadadze & M. Porrati, *Phys. Lett. B* **484**, (2000) 112 hep-th/0002190, *Phys. Lett. B* **484**, (2000) 129, hep-th/0003054, *Phys. Lett. B* **485**, (2000) 208, hep-th/0005016.
- [15] P. Kanti, K.A. Olive & M. Pospelov, PRD **62**, (2000) 126004, hep-ph/0005146, P. Binétury, C. Deffayet & D. Langlois, *Nucl. Phys. B* **565**, (2000) 269, hep-th/9905012, P. Kanti, I.I., Kogan I.I., K.A. Olive & M. Pospelov, *Phys. Lett. B* **468**, (1999) 31, hep-ph/9909481, *Phys. Rev. D* **61**, (2000) 106004, hep-ph/9912266; C. Csaki *et al.*, *Phys. Rev. D* **62**, (045015) 2000, hep-ph/9911406, H. Ziaepour, hep-ph/0010180 (examples of early works); V. Sahni, astro-ph/0502032 (review).
- [16] J. Middleditch, astro-ph/0608386.
- [17] A.G. Riess, M. Livio, astro-ph/0601319.
- [18] A. Gal-Yam, D. Maoz, *MNRAS* **347**, (2004) 942, astro-ph/0309796.
- [19] F. Simpsso, S. Bridle, *Phys. Rev. D* **73**, (2006) 083001, astro-ph/0602213.
- [20] M. Sako, *et al.*, astro-ph/0504455.
- [21] A. Shafieloo, *et al.*, *MNRAS* **366**, (2006) 1081, astro-ph/0505329.
- [22] A.R. Knop *et al.*, *ApJ*. **598**, (2003) 102, astro-ph/0309368.
- [23] W.H. Press, *et al.*, “Numerical Recipes in C”, Cambridge University Press.